S. Masuzaki et al.

Analyses of Structure, Composition and Retention of Hydrogen Isotopes in the JET-ILW Divertor Tiles

Preprint of Paper to be submitted for publication in Proceeding of 16th International Conference on Plasma-Facing Materials and Components for Fusion Applications

Analyses of Microstructure, Composition and Retention of Hydrogen Isotopes in Divertor Tiles of JET with the ITER-Like Wall

S Masuzaki[1,2], M Tokitani[1,2], T Otsuka[2], Y Oya[3], Y Hatano[4], M Miyamoto[5], R Sakamoto[1,2], N Ashikawa[1,2], S Sakurada[3], Y Uemura[3], K Azuma[3], K Yumizuru[4], M Oyaizu[6], T Suzuki[6], H Kurotaki[6], D Hamaguchi[6], K Isobe[6], N Asakura[6], A Widdowson[7], K Heinola[8], S Jachmich[9], M Rubel[10] and JET contributors*

[1]*National Institute for Fusion Science, Oroshi 322-6, Toki 509-5292, Japan*
[2]*SOKENDAI (The Graduate University for Advanced Studies), Oroshi 322-6, Toki 509-5292, Japan*
[3]*Kindai University, 3-4-1 Kowakae, Higashiosaka, Osaka 577-8502, Japan*
[4]*Shizuoka University, Shizuoka, 422-8529, Japan*
[5]*University of Toyama, Gofuku 3190, Toyama 930-8555, Japan*
[6]*Shimane University, Matsue, Shimane 690-8504, Japan*
[7]*National Institutes for Quantum and Radiological Science and Technology (QST), Rokkasho Aomori 039-3212, Japan,*
[8]*Culham Centre for Fusion Energy, Culham Science Centre, Abingdon, OX 14 3DB, UK*
[9]*University of Helsinki, Box 43, FIN-00014 Helsinki, Finland*
[10]*Association Euratom-Etat Belge, ERM-KMS, Brussels Belgium*
[11]*Royal Institute of Technology (KTH), 100 44 Stockholm, Sweden*

Abstract

Results of the comprehensive surface analyses of divertor tiles and dusts retrieved from JET after the first ITER-like Wall campaign (2011-2012) are presented. The samples cored from the divertor tiles were analyzed. Numerous nano-size bubble-like structures were observed in the deposition layer on the apron of the inner divertor tile, and a beryllium dust with the same structures were found in the matter collected from the inner divertor after the campaign. This suggests that the nano-size bubble-like structures can make the deposition layer to become brittle and may lead to cracking followed by dust generation. X-ray photoelectron spectroscopy (XPS) analyses of chemical states of species in the deposition layers identified the formation of beryllium-tungsten intermetallic compounds on an inner vertical tile. Different tritium retention profiles along the divertor tiles were observed at the top surfaces and at deeper regions of the tiles by using the imaging plate technique.

Keywords: JET, ITER-Like Wall, divertor, fuel retention, dust, XPS

PACS: 52.40 Hf

Corresponding author: Suguru Masuzaki, masuzaki@LHD.nifs.ac.jp

1. Introduction

In fusion devices, material migration with erosion and deposition of the surfaces of the plasma facing components (PFCs) in the vacuum vessel, and hydrogen isotopes retention in such components are crucial for the overall plasma performance. Understanding of the material migration and the hydrogen isotopes retention are necessary for exploitation of future fusion devices such as ITER and DEMO. For example, the ITER operation time will be limited by tritium inventory and dust accumulated inside the vacuum vessel [1].

In order to improve understanding of wall material impact on plasma performance and to prepare for campaigns in ITER the JET tokamak has been operated since year 2011 with the ITER-like Wall (JET-ILW) [2]. Plasma-facing materials in that experiment are: beryllium (Be) in the main chamber wall, and tungsten (W) in the divertor, i.e., the same materials as in the current ITER design [3]. Three ILW campaigns conducted in 2011 - 2012, 2013 - 2014 and 2015 -2016 have been followed by broad studies of PFC removed from the vacuum vessel after each period. This article provides an account on comprehensive analyses of the divertor tiles after the first campaign (ILW-1) conducted at the International Fusion Energy Research Centre (IFERC), National Institutes for Quantum and Radiological Science and Technology (QST), Rokkasho, Japan in the framework of the Broader Approach activities. Material research facilities at IFERC are certified for work with beryllium- and tritium-contaminated specimens. The surface microstructures of the divertor tiles from JET have been examined with scanning electron microscopy (SEM) and transmission electron microscopy (TEM). Further, the surface compositions have been analyzed with energy dispersive X-ray spectroscopy (EDS), electron probe micro analysis (EPMA) and X-ray photoelectron spectroscopy (XPS), while the retention of hydrogen isotopes has been assessed by thermal desorption spectroscopy (TDS) and imaging plate (IP) technique.

2. Description of analyzed samples

Figure 1 shows a poloidal cross-section of the JET divertor in ILW-1. Typical plasma configurations in the divertor are also shown. In the most frequent case the inner and outer strike points were located on Tiles 3 and 5, respectively [4]. The divertor tiles are made of W coated carbon fiber composite material (CFC), except for Tile 5, which is made of bulk W [4, 5]. In the standard case, CFC substrate is coated by magnetron plasma with 20 μm of W on a molybdenum (Mo) interfacial layer [6]. Some marker tiles were installed to determine erosion-deposition of PFC. In the marker tiles the thickness of the W coating was about 18

μm covered with approximately 3 μm of Mo layer and approximately 3 μm thick W layer [7]. Further, in markers on Tile 3, the outermost 3 μm W coating was not applied, thus leaving Mo as the plasma-facing material to enable the investigation of W deposition in ILW-1 [4].

For post mortem analyses, the W/CFC tiles were cored to obtain samples 17 mm in diameter and 5 mm in thickness. Twenty one samples were selected for the work reported below. Their positions are shown by the small rectangles in the six tiles in Figure 1. Although all six tiles are in a poloidal cross-section in Figure 1, Tiles 1, 3 and 4 were retrieved from the toroidal section of 14, and Tiles 6, 7 and 8 were retrieved from the toroidal section of 2, respectively. The notation of the samples shows the tile number from which each sample was cored (the number to the left of the slash mark), and poloidal position of each sample on the tile (the number to the right of the slash mark) as summarized in Table 1. In Table 1, "S-coordinate" system is the poloidal position on the divertor tile surfaces. The origin of the system is the edge of the inner apron tile (Tile 0) next to Tile 1 in Fig. 1 (not shown) [8]. The first step in the study was the measurement of tritium with the IP technique. Afterwards, each disk shape was sectioned into four pieces in order to provide samples for examination with various microscopy and spectroscopy methods as shown in Table 1.

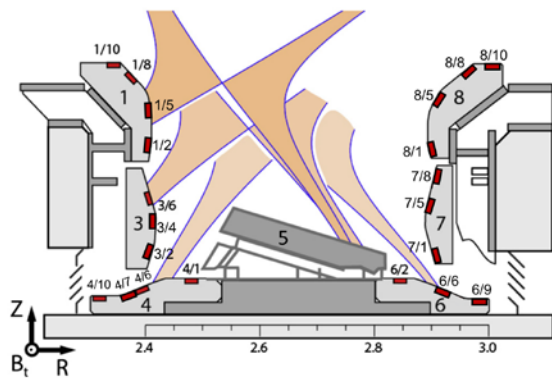*Fig. 1. A poloidal cross-section of the JET divertor with three typical plasma configurations in ILW-1, and positions of the analyzed samples, which are shown by the small rectangles. The notation of the samples show the tile number from which each sample was cored (the number to the left of the slash mark), and poloidal position of each sample on the tile (the number to the right of the slash mark).*

Table 1. Sample positions and the results of analyses shown in this paper. "S-coordinate" system is the poloidal position on the divertor tile surfaces. The origin of the system is the edge of the inner apron tile (Tile 0) next to Tile 1 in Fig. 1 (not shown) [8].

Tile	Sample	Position of samples (s-coordinate, mm)	SEM TEM	XPS	TDS	IP
1	1/10	Apron part (218)	✓		✓	✓
	1/8	Upper part (262)		✓	✓	✓
	1/5	Intermediate part (331)				✓
	1/2	Lower part (392)			✓	✓
3	3/6	Inner strike point (485)		✓	✓	✓
	3/4	Inner strike point (527)				✓
	3/2	Inner strike point (565)	✓		✓	✓
4	4/10	Shadowed part (735)	✓		✓	✓
	4/7	Slope part (797)				✓
	4/6	Slope part (818)		✓	✓	✓
	4/1	Shadow of Tile 5 (917)			✓	✓
6	6/2	Shadow of Tile 5 (1351)			✓	✓
	6/6	Slope part (1437)	✓	✓	✓	✓
	6/9	Shadowed part (1492)			✓	✓
7	7/1	Outer strike point (1642)		✓	✓	✓
	7/5	(1734)				✓
	7/8	(1796)				✓
8	8/1	Lower part (1829)				✓
	8/5	Intermediate part (1912)				✓
	8/8	Upper part (1967)				✓
	8/10	Apron part (2023)		✓	✓	✓

3. Results and discussion

3.1. Microstructure of deposition layer and its effect on dust generation

For the microstructure observation with TEM, the samples were fabricated by using focused ion beam (FIB) to make cross-sections in the form of thin lamellae. The microstructure determined by TEM for the inboard-side tiles samples 1/10, 3/2 and 4/10 has been reported in [9]. On samples 1/10 and 4/10 there were deposited layers of stratified structure and the total thicknesses of ~1.5 μm and 200-300 nm, respectively. They consist of layers rich either in high-Z atoms (darker areas) or low-Z species, as shown in Figure 2(a).

In the deposited layer on 1/10, numerous nano-size bubble-like structures have been found, as shown in Figure 2(a), and the biggest size is over 100 nm. On the contrary, in the layer on sample 4/10, structures of that kind have not been detected. Such structures can make the

deposit very brittle and, as a consequence, this may lead to the layer cracking and dust generation.

Dust particles discussed in the following were collected by vacuum cleaner from the inner divertor [10]. Figure 2(b) shows the entire dust particle, and a bright field TEM image of a cross-section of the dust fabricated with FIB. The main component of the dust is Be as inferred from the electron diffraction pattern. Numerous bubble-like structures up to several 100 nm in size are in the dust, as shown in Figure 2(c), which is a magnification of the rectangular part in Figure 2(b). This is the first observation of dust with such microstructure. Dust of this kind is considered to be generated by cracking and peeling-off of co-deposited layers.

A stratified structure of the deposits has been also observed at the sloping part of Tile 6. It may be suggested that this can be a common feature of the deposits on the divertor tiles after the ILW-1 operation. This statement is restricted to that campaign, because mixed stratified, columnar and porous structures of deposits have been identified following ILW-2 [11]. The nano-size bubble-like structures were observed only in the deposition layer on 1/10, which is from an inner apron tile at this stage. As discussed in reference [9], the bubble-like structures may be trap sites of hydrogen isotopes and may be related to the locally enhanced deuterium at this position which is observed in reference [12] and is mentioned below in this study.
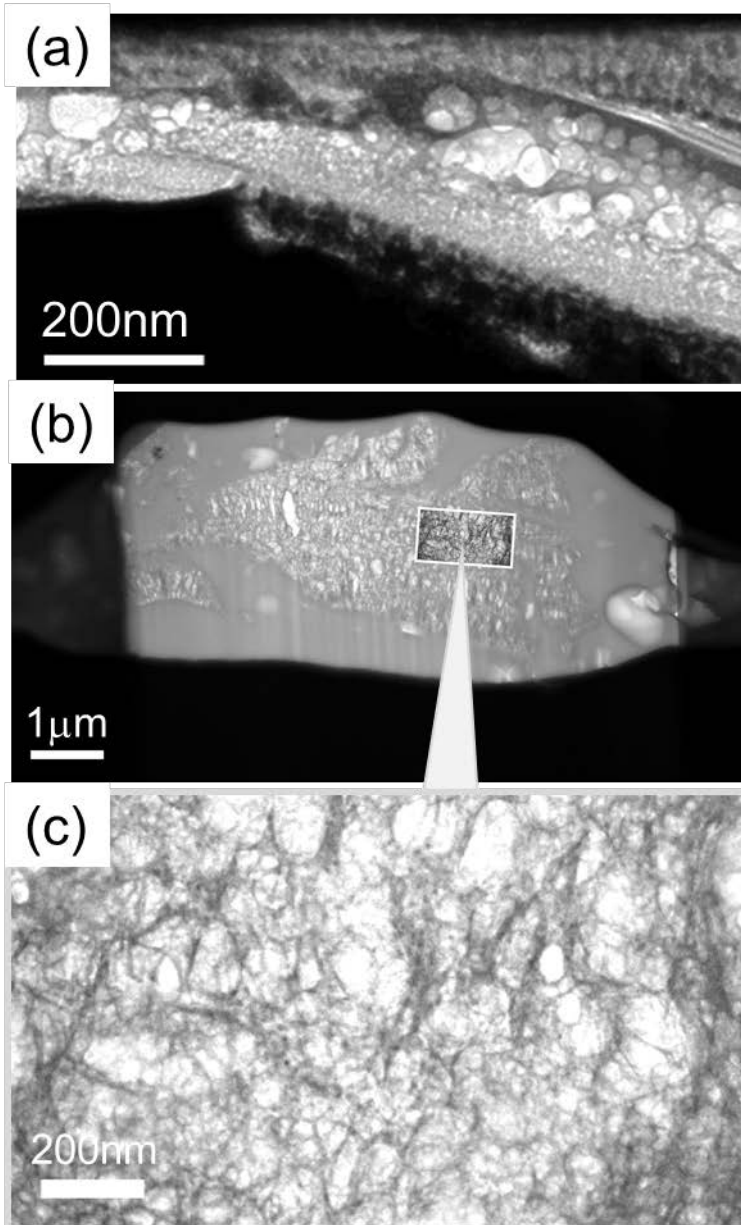
Figure 2. (a) Cross-sectional bright field transmission electron microscope (TEM) image of the near surface of 1/10 sample [9]. The bottom black area is original W coating, and the deposition area appear on the W coating. In the deposition area, the bright part shows the low-Z material, low density or thinner part. Bright round parts are the bubble-like structures. (b) Cross-sectional bright field TEM image of the entire dust. The bottom black area is the indium disk on which the dust was placed. The homogeneous grey area is oil-based ink which was used for surface protection against the focused ion beam (FIB). (c) A magnified view of the region drawn from the white rectangular region in (b). As in (a), the bright round parts are the bubble-like structures.

3.2. Atomic composition analysis of the surface and the deposition layer

Surface composition of the divertor tiles has been reported earlier following analyses conducted by means of standard and micro-beam Rutherford backscattering (RBS) and nuclear reaction analysis (NRA), and also by secondary ion mass spectroscopy (SIMS) [7, 8, 12, 13]. At IFERC, EDS and EPMA were applied to determine the samples' composition [9]. Cross-sections of 1/10, 3/2 were analyzed. W, carbon (C), oxygen (O), Mo and beryllium (Be) were detected in the deposition layer on 1/10 [9]. On Tile 3 coated originally with Mo, that element is still present after the plasma exposure on sample 3/2 which was cored from the erosion zone thus suggesting that the layer has not been fully eroded. Mo coexists with Be, but it is not possible to determine the state of that layer whether an intermetallic compound or a mixture of co-deposited elements which are Be from the plasma flux and are promptly re-deposited Mo.

In this study, depth profiles of atomic composition of the tile samples from the inner (1/8, 3/6, and 4/6) and outer divertor tiles (6/6, 7/1, and 8/10) were analyzed by using XPS (Ulvac-Phi inc. PHI 5000 VersaProbe II) assisted by surface sputtering with argon ion (Ar^+) beam (1 keV, ~ 6.25×10^{17} ions/m^2s). The monochromatic X-ray source (Al Kα, 1486.6 eV) was utilized. The analyzed area was ~ 100 μm of diameter, and the sputtering time was up to 20 minutes. From the rough estimation, in which W target is assumed, the depth is less than 100 nm with 20 minutes sputtering, though the accurate depth estimation unfortunately could not be conducted because there is no laser profilometer or stylus equipment in the controlled area at IFERC. It may also be stressed that the original surface roughness of W-coated CFC tiles would make the depth determination difficult.

In the surface region of samples 1/8 and 6/6 W is the dominant component. In the case of sample 1/8, Be, C, O and Al were observed. W and Al contents increase with depth while amounts of other species decrease with depth. This profile is similar to that measured by SIMS at the apron part of Tile 1 [7]. On sample 6/6, W, O and C are observed. Be concentration is much smaller than that of W, O and C. And W concentration is much larger than that for other elements. The result of the analysis of deposition and erosion on the divertor tiles with RBS shows homogeneous W deposition on Tile 6, and net erosion of W on Tile 5, which is a bulk tungsten tile [4]. The result of the XPS in this study is consistent with the result of the analysis with RBS. The source of W might be Tile 5 on which the outer strike point was placed most frequently, though the W transport mechanism, which made the homogeneous W deposition on Tile 6, has not been cleared [4]. Indeed, a stepwise transport

(erosion – prompt deposition – re-erosion and re-deposition) during discharges may be considered as an important mechanism of the W transport [14, 15].

In sample 7/1 the dominance of W in the surface layer is detected. Profiles of O and C decrease steeply with depth. The outer strike point was sometimes located on 7/1 and erosion is considered to be dominant at that position [4]. On the other hand, as mentioned above, the W from Tile 5 could deposit on the position of sample 7/1 with stepwise transport.

The depth profiles of atomic composition on samples 3/6 and 4/6 are similar to each other, except for Mo which is the top surface material on Tile 3. In both cases, C, W, O, and Be are observed, and their amounts are similar for these samples. C is a dominant component with a share of ~ 40 %, the amounts of W and O are 20-26 %, and Be is on the level of ~ 10 %. On 3/6, the amount of Mo is almost the same as Be, while the share of Mo is less than 1% in other samples. The inner strike point was frequently at the position of 3/6, and sometimes near the position of 4/6 [4]. The result suggests that the formation of modified surface layers was similar at the two positions.

On 8/10, O, W, C and Be were observed with the dominance of oxygen: around 40%, while the amounts of W, C, and Be were almost equal at around 20 %. Al was detected except for 6/6 and 7/1. The amount of Al is up to 9 % in 1/8 and in other samples the concentration is 1-3 %. One of the possible sources of Al is electric insulator (Al_2O_3), which has been used in JET. The results of XPS analyses are not fully consistent with the results in previous studies. For example, a much larger content of Be was observed in previous studies [4, 7, 8, 13]. This may be related to non-uniform distribution of species [12] even in samples originating from similar regions on the tiles. This feature may play a role when analyses are carried out on small areas, such as 100 μm of diameter in the case of XPS.

3.3. Chemical state of deposits

The chemical states of species in deposits on 1/8, 3/6, 4/6, 6/6, and 8/10 were analyzed with the sputter-assisted XPS. Plots in Figure 3 represent the change of core level values of W $4f_{7/2}$, C 1s, and O 1s with depth in four samples. The obtained profiles are in two categories: static and dynamic. The difference of them is whether the depth profiles of chemical shifts in binding energies change largely (dynamic type) or not (static type). This means that the chemical states have depth dependence in the dynamic type. For the 1/8 and 6/6 cases, the shift of binding energy of W $4f_{7/2}$ and C 1s changes largely within the analyzed depth, thus 1/8 and 6/6 are dynamic type. In other cases, changes of the binding energies are not

significant thus suggesting that they are in the static type. In the dynamic type case, the changes of chemical states may be caused by the change of plasma condition during subsequent operation periods.
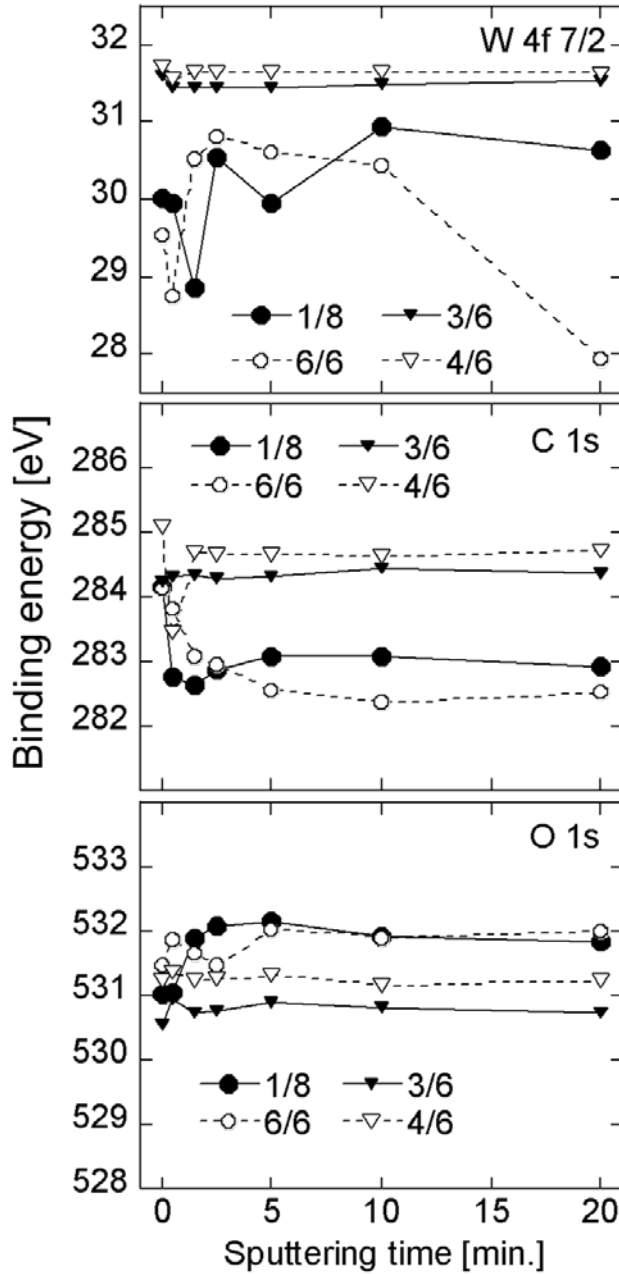

Figure 3. Depth profiles of binding energies shifts for W 4f$_{7/2}$, C 1s and O 1s on the samples of 1/8, 3/6, 4/6, and 6/6, respectively, measured by using X-ray photoelectron spectroscopy (XPS) with Ar$^+$ beam sputtering. Depth is shown by using sputtering time.
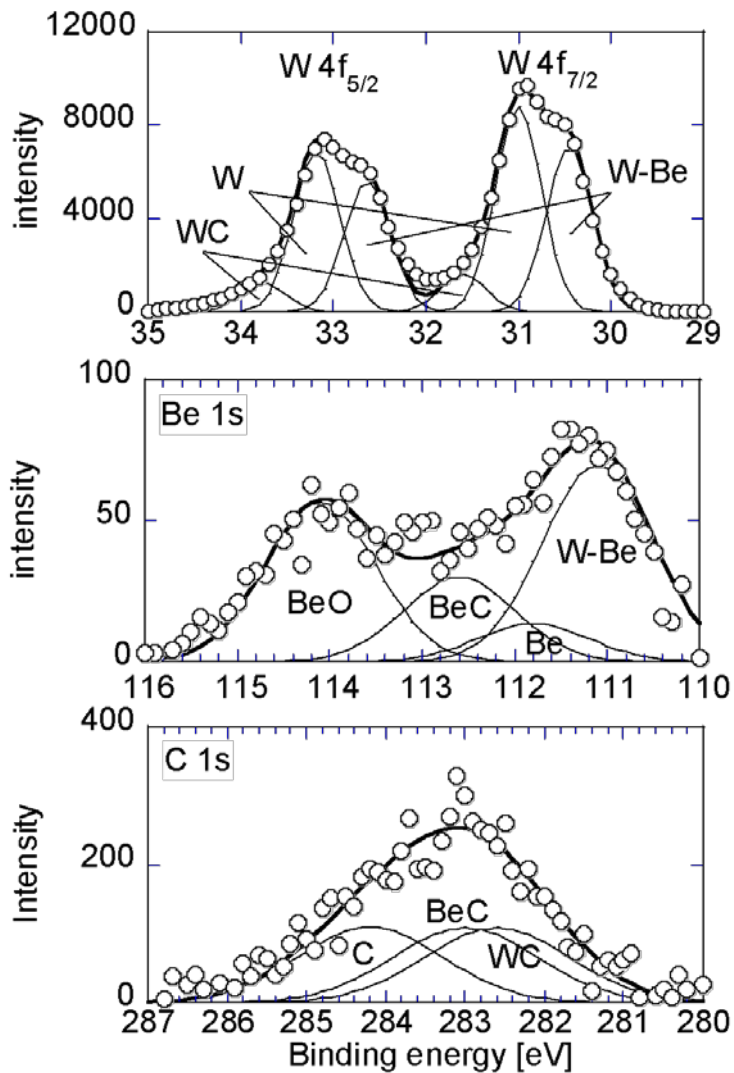
Figure 4. W 4f (top), Be 1s (middle), and C 1s (bottom) XPS spectra for the sample of 1/8 after 10 minutes sputtering with Ar ion beam. For all cases, linear backgrounds were subtracted. Results of the peak separation for each spectrum were also shown. Bold lines show the sums of components.

With regard to Be, results of XPS analysis indicate the presence of BeO rather than metallic Be, except for samples 1/8 and 6/6 where the shifts of binding energies are very large. The core level spectra W 4f, Be 1s, and C 1s on 1/8 after 10 minutes sputtering are shown in Figure 4. For all cases, linear backgrounds were subtracted. There are shoulders at lower energy side of W 4f spectra. These shoulder structures are considered to be the sign of W-Be compounds formation [16], and that has not been clearly detected in other samples at this stage. Peak separation was conducted for the spectra as shown in Figure 4. Gaussian fitting was applied with fixed binding energies for metallic W $4f_{7/2}$ (31 eV) and $4f_{5/2}$ (33.28 eV), metallic Be (111.8 eV) and BeO (114.1 eV). It was considered that in both W and Be cases,

carbide could be formed. For the carbides, binding energies of WC (31.6 eV and 33.78 eV) and BeC (112.6 eV) were assumed. For W-Be compounds, binding energies of 30.45 eV and 32.63 eV for W 4f, and 111.1 eV for Be were assumed. For C 1s case, binding energies of graphite (284.2 eV), WC (282.6 eV), and BeC (283 eV) were assumed. As the results, the experimental data of the spectra could be reproduced as shown in Figure 4. It should also be stressed that the formation of W_2C compound on the JET ILW divertor tiles (Tile 4, 6, 7 and 8) has been proven by X-ray Diffraction (XRD) analysis [17].

3.4. Hydrogen isotopes retention analysis with TDS

Evaluation of the amounts of retained D in the divertor tiles has been carried out with TDS at IFERC for samples of 1/10, 1/8, 3/2, 4/6, 6/2, 6/6, 7/1 and 8/10. The desorption was performed up to the temperature of 1273 K with a heating rate of 0.5 K/s by using an infrared-gold-image furnace. The evolution of H_2 (mass 2), HD (mass 3) and D_2 (mass 4) was measured using two quadrupole mass spectrometers (MKS Microvision, 1-6 amu, and 1-200 amu). There was an attempt to determine also the tritium release (mass 6, T_2) but the signal was below the sensitivity level. Figure 5(a) shows the profile of the deuterium concentration along the poloidal cross-section of the divertor represented by the S-coordinate [8]. The data obtained in this study at IFERC are plotted by the open squares, while the data of earlier measurements [8] are plotted by the closed squares. The concentration of D measured in this study is in general agreement with that determined in the previous study. However, the difference is observed for Tile 1, where the concentrations obtained in this study are about one order of magnitude lower than those measured and reported in [8]. This is possibly attributed to the difference of the thickness of deposition layer. As mentioned in section 3.1, the thickness of the deposits on the apron part of Tile 1 (sample 1/10) was estimated by SEM to be ~ 1.5 μm [9], while there were also reports of a ten times greater thickness [7, 18]. The sample analyzed in this study was cored from the region near the edge of Tile 1, thus the shadowing effect by the neighbor tile could occur.
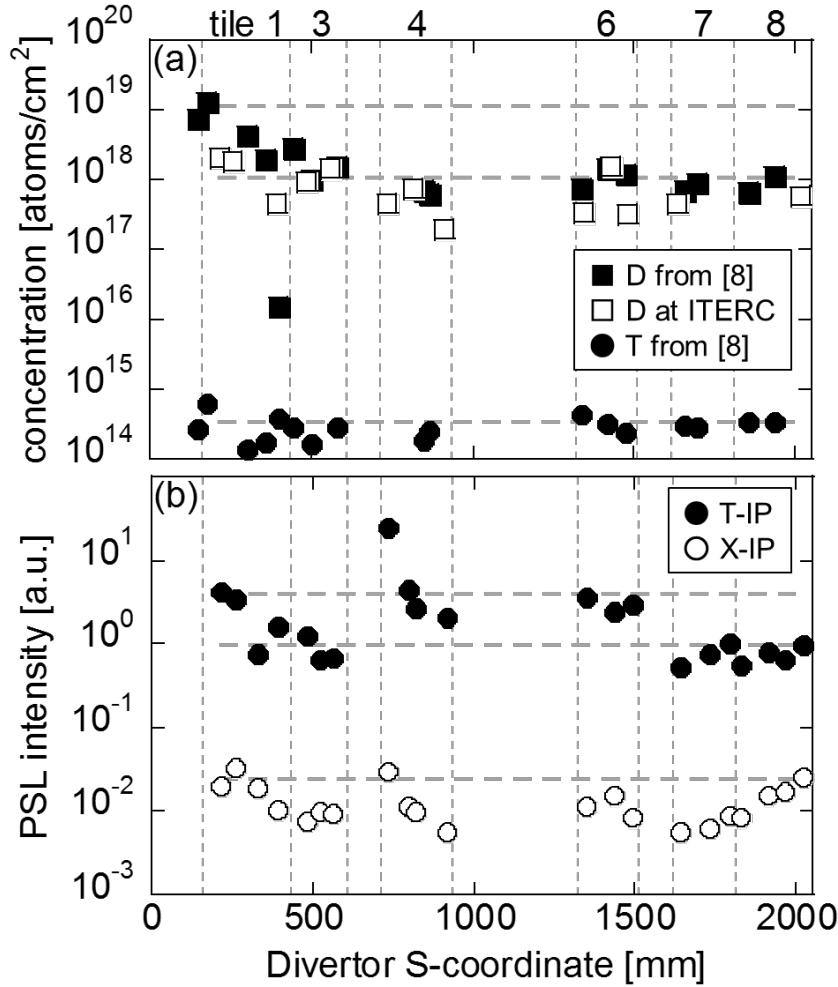
Figure 5. (a) Atomic concentration profiles of deuterium and tritium measured with thermal desorption spectroscopy (TDS). The TDS data shown by closed symbols are the same as the data in ref [8], and open squares are the data obtained at IFERC. (b) Photo-stimulated luminescence (PSL) intensity profiles of the two types of Imaging Plates (T-IP and X-IP, see section 3.5) along the divertor S-coordinate. The horizontal dashed lines are to mark the differences of values between at the in- and out-board divertor tiles.

3.5. Measurement of retained tritium

Tritons are produced by DD fusion reactions with the energy of 1.01 MeV. In the JET case, many of the tritons escape from the confinement region without large loss of energy, and they are implanted in PFCs. A part of the generated tritons is thermalized in the plasma and reach the PFCs with the same temperature as the background plasma. As a result, there are deep and shallow ranges of the incident T in the divertor tiles corresponding to the high incident energy (up to 1.01 MeV) and the low (thermalized) incident energy, respectively. To compare the distributions of T reaching the divertor tiles with the different incident energy ranges, IP

technique was used to measure the retained T in the divertor tiles. Two types of IP, BAS IP TR and BAS IP MS (GE Healthcare), were utilized. BAS IP TR has sensitivity to the low energy β-electrons generated by β decay of T (5.7 keV in average, 18.6 keV in maximum). On the other hand, BAS IP MS has a protection film which completely shields the low energy β-electrons, and that was used for the detection of X-rays induced by the emitted β-electrons from T in the tiles. Hereafter in this article, BAS IP TR is called T-IP (IP for tritium) and BAS IP MS is called X-IP (IP for X-ray). The range of the β-electrons from T in metals is around 1 μm, which is much smaller than the range of the bremsstrahlung X-ray induced by the emitted β-electrons from T. That means the T-IP can only measure shallow incident T with low incident energy, and the X-IP can measure deep incident T with high incident energy.

In this study, T-IP and X-IP were exposed to the sample surfaces with a face to face contact for 2 h and for 70 h, respectively. After the exposure, the photo-stimulated luminescence (PSL) intensities from the IPs, corresponding to T amount, were obtained by using a laser scanner (FLA-7000). Figure 5 (b) shows the PSL intensity profiles for T-IP and X-IP along the divertor S-coordinate. For the case of T-IP the intensities at the inner vertical tiles (Tiles 1, 3) are larger than those at the vertical tiles from the outer divertor (Tiles 7, 8). That profile is similar to the profile of the atomic concentrations of deuterium obtained with TDS, as shown in Figure 5(a). This result is consistent with the result in earlier studies with T-IP [18, 19].

On the other hand, for the case of X-IP, the PSL intensities at the inner and outer vertical tiles are similar. With regard to the T concentration profile obtained with TDS in Figure 5(a), the concentrations at the inner and outer vertical tiles are also similar as the PSL intensity profile for X-IP. The T concentration obtained with TDS is considered to include both shallow and deep incident T. Therefore, the similarity of the profiles of PSL intensity for X-IP and T concentration obtained with TDS suggests that the high energy triton is the major component of the retained T in the divertor tiles. For the detailed comparison between the distributions of retained T and the high energy tritons lost to wall, performing the simulation of high energy triton, e.g., by the Monte Carlo fast ion code ASCOT [21], is necessary.

In Figure 5(b), for both T-IP and X-IP, the PSL intensities on Tile 4 increase when approaching the shadowed regions in the divertor (see Figure 1). The intensities at sample 4/10 were the largest in each PSL intensity profile. It should be noted that the D retention at this position is not so large compared to D retention at other positions as shown in Figure 5(a). The difference in the relative amounts of D and T at this position are not yet understood.

4. Summary

Comprehensive analyses of the divertor tiles and dusts retrieved from JET after the first ILW campaign conducted at IFERC, in the framework of Broader Approach led to the detailed determination of the microstructure of the deposition layer and of the dusts, surface composition including chemical states of the species, and the retention of hydrogen isotopes. Observation of deposits and dusts with TEM suggested a possible dust generation mechanism which relates to particle induced material damage. Surface composition and chemical states were analyzed by using XPS, and the depth profiles of the binding energies in deposition layers on the divertor tiles were obtained. Comparison of the deuterium retention profile along the divertor tile surfaces obtained by using TDS between this and a previous study [8] shows good agreement. Results of the analysis of tritium retention profile along the divertor tile surfaces with two types of IP show the different profiles of tritium with different incident energy ranges.

In the deposition layer on the apron part of Tile 1, the regions with nano-size bubble-like structures are detected. Similar structures have been identified in the beryllium dust collected from surfaces of the inner divertor tiles. This suggests that bubble-like structures can make the deposition layer brittle, and this may lead to dust generation.

XPS examination of the composition and chemical state analyses has revealed static and dynamic types of deposition layers. In the static type, the changes of chemical states of deposits are small, whereas in the other type large changes of the chemical states of deposits occur. Be appears in deposits mainly in the form of BeO, except for samples 1/8 and 6/6 on which the depth profiles of chemical shifts in binding energies change largely. An indication of W-Be compounds formation has also been found at the inner vertical divertor tile. The melting points of W-Be compounds are much less than that of W, and thus the condition of the formation of the compounds should be revealed.

Analysis of tritium retention revealed two types of profiles corresponding to the thermalized tritium co-deposited in the surface layer and not confined tritium implanted with high energy at a deeper region. The profile of the thermalized tritium is similar to the retention profile of deuterium. The profile of high energy tritons is in-out symmetrical in the divertor tiles.

It should be stressed that the investigations with XPS and two types of imaging plate have been conducted for the first time for materials retrieved from JET-ILW. These investigation create the basis for the future examination of materials after the third experimental ILW

campaign where high power operation was performed and large amounts of nitrogen were used for edge cooling.

References

[1] Shimada M *et al* 2013 *J. Nucl. Mater.* **438** S996

[2] Matthews G F *et al* 2011 *Phys. Scr.* **T145** 014001

[3] Pitts R A *et al* 2013 *J. Nucl. Mater.* **438** S48

[4] Mayer M *et al* 2016 *Phys. Scr.* **T167** 014051

[5] Rubel M *et al* 2013 *J. Nucl. Mater.* **438** S1204

[6] Ruset C *et al* 2009 *Fusion Eng. Des.* **84** 1662

[7] Coad J P *et al* 2014 *Phys. Scr.* 2014 **T159** 014012

[8] Heinola K *et al* 2016 *Phys. Scr.* **T167** 014075

[9] Tokitani M *et al* 2017 *Fusion Eng. Des.* **116** 1

[10] Widdowson A *et al* 2014 *Phys. Scr.* **T159** 014010

[11] Fortuna-Zalesna E *et al.* ”Studies of dust from JET with the ITER-Like Wall: Composition and internal structure”, *Nucl. Mater. Energy,* http://dx.doi.org/10.1016/j.nme.2016.11.027

[12] Bergsåker H *et al* 2015 *J. Nucl. Mater.* **463** 956

[13] Brezinsek S *et al* 2015 *J. Nucl. Mater.* **463** 11

[14] D. Naujoks and R. Behrisch 1995, *J. Nucl. Mater.* **220-222** 227

[15] M. Rubel *et al* 2013, *J. Nucl. Mater.* **438** S170

[16] Wiltner A and Linsmeier Ch 2006 *New J. Phys.* **8** 181

[17] A. Lagoyannis *et al* 2017, *Nucl. Fusion* **57** 076027

[18] Baron-Wiechec A *et al* 2015 *J. Nucl. Mater.* **463** 157

[19] Hatano Y *et al* 2015 *J. Nucl. Mater.* **463** 966

[20] Hatano Y *et al* 2016 *Phys. Scr.* **T167** 014009

[21] Hirvijoki E *et al* 2014 *Computer Physics Communications* **185** 1310